Modeling Traffic Jams in Extracellular Transport in Axons

Jan Habscheid

Abstract

A frequent reason for neurodegenerative diseases is the swelling of axons (nerve cells). This swelling is often caused by traffic jams in intracellular traffic. This work inspects a mathematical model, combining diffusive and advective transport behavior, for intracellular traffic. This coupled model describes the natural movement of free particles and particles riding on microtubules towards and away from the neuron body and the interaction between these different particles.

This work aims to understand how to model diffusive and advective transport both, analytically and numerically. Furthermore, it tries to understand circumstances for traffic jams with possible solutions to prevent those. Finally, it suggests two, theoretical, possibilities to reduce and prevent traffic jams in nerve cells from a medical point of view.

Index Terms

Intracellular Traffic, Upwind-Method, Diffusion, Advection, Method of Characteristics

1 Introduction

Neurodegenerative diseases are a serious threat to humans health. One reason for these diseases is the swelling of axons, caused by irregularities in intracellular traffic in the the axons. Axons are a part of neurons, transmitting an electrical signal (compare with Figure 1.1). These axons can be up to one meter in the human body and support little synthesis. Therefore, certain materials have to be from the cytoplasm of the cell body. Diffusive transport is not fast enough to transport the needed materials, which leads to an additional advective transport where particles attach themselves to molecular motors (compare with [2]).

This work will investigate the transport in the axons by investigating a mathematical model proposed in [2]. The investigation aims to learn about certain challenges on how to solve advection equations numerically, understand the transport behavior in axons, identify possible problems for our nerves and understand why and under what circumstances traffic jams can occur in the axons. A traffic jam is a situation where particles accumulate along the spatial domain and hinder an efficient transport mechanism.

Therefore, the problem to be solved is a coupled system of partial differential equations, consisting of one diffusion and two advection equations. It reads:

Date: 05.02.2025,
Referee: Steinar Evje
Author: Jan Habscheid, J.Habscheid@stud.uis.no, Student ID: 287338

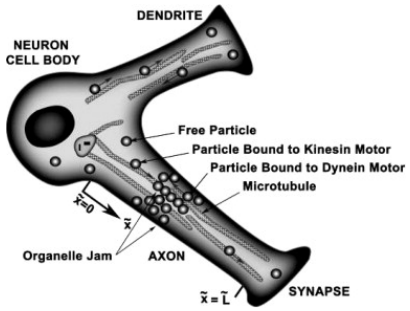

Figure 1.1: Schematic view of the neuron cell body (see [2]) Axons transmit an electrical signal and support little synthesis. Therefore, the needed materials are transported via diffusion and advection.

$$\underbrace{\hat{n}_{\hat{t}}}_{1.A} = \underbrace{\hat{D}_0 \hat{n}_{\hat{x}\hat{x}}}_{1.B} - \underbrace{(1+\hat{k}_-)\hat{n} + \hat{k}_p \hat{n}_+ + \hat{k}_n \hat{n}_-}_{1.C} \tag{1.1}$$

$$\underbrace{(\hat{n}_+)_{\hat{t}}}_{2.A} + \underbrace{\left(\frac{V_+}{V_{+,0}}\hat{n}_+\right)_{\hat{x}}}_{2.B} = \underbrace{\hat{k_+}\hat{n} - \hat{k}_p \hat{n}_+}_{2.C} \qquad \hat{x} \in [0, \hat{L}] \tag{1.2}$$

$$\underbrace{(\hat{n}_-)_{\hat{t}}}_{3.A} + \underbrace{\left(\frac{V_-}{V_{+,0}}\hat{n}_-\right)_{\hat{x}}}_{3.B} = \underbrace{\hat{k}_- \hat{n} - \hat{k}_n \hat{n}_-}_{3.C} \tag{1.3}$$

with free particle concentration $\hat{n}$ and $\hat{n}_\pm$ the concentration of particles moving in positive/negative direction. The spatial domain is described by $\hat{x} = [0, L]$ on a timeframe of $[0, t_{\text{end}}]$. Furthermore, $\hat{D}_0$ is the diffusion coefficient, $V_\pm$ the molecular motor velocity along microtubules regarding the $\pm$ direction, $V_{\pm,0}$ molecular velocity along microtubules regarding $\pm$ direction in the case that the concentration of molecules riding on microtubules is very low, the rate coefficients $\hat{k}_p, \hat{k}_n, \hat{k}_+$ and $\hat{k}_-$.

Equation 1.1 describes the movement from free particles by diffusion. The temporal change is described by term 1.A and the diffusive behavior by 1.B. The source term 1.C describes the exchange of particles with $\hat{n}_\pm$. The two advection equations 1.2 and 1.3 describe the movement of particles moving in positive and negative direction due to convection. The terms 2.A and 3.A describe the temporal change, and 2.B and 3.B the advective behavior. Both equations also have some exchange of concentration with the other particles, described by terms 2.C and 3.C.

Equations 1.2 and 1.3 can be reformulated into a generic advection equation of the form

$$u_t + a(x,t)u_x = q(x,t,u) \tag{1.4}$$

with the advection velocity a, the property of interest u and the source term q. This results in

$$u_{t,2} = (\hat{n}_+)_{\hat{t}}\,, \quad a_2(x,t) = \frac{V_+}{V_{+,0}}, \quad u_{x,2} = \hat{n}_{+,\hat{x}}, \quad q_3(x,t,u) = \hat{k}_p\hat{n} - \hat{k}_p\hat{n}_+ \tag{1.5}$$

$$u_{t,3} = (\hat{n}_-)_{\hat{t}}\,, \quad a_3(x,t) = \frac{V_-}{V_{+,0}}, \quad u_{x,3} = \hat{n}_{-,\hat{x}}, \quad q_3(x,t,u) = \hat{k}_-\hat{n} - \hat{k}_n\hat{n}_- \tag{1.6}$$

Therefore, it is sufficient to know how to deal with a generic advection equation in the form of equation 1.4 to solve the two advection equations, describing the particle transport in axons, both analytically and numerically.

2 Theory and Methods

2.1 Dimensionless Properties

Dimensionless quantities are introduced in the following to scale the physical values to some reference level. The dimensionless quantities are defined as follows (compare with [2])

$$\hat{x} = \frac{xk_+}{V_{+,0}}, \qquad \hat{t} = tk_+, \qquad \hat{D}_0 = \frac{D_0 k_p}{V_{+,0}^2}, \qquad \hat{n} = \frac{nV_{+,0}^3}{k_+^3}, \quad n_\pm = \frac{\hat{n}_\pm V_{+,0}^3}{k_\pm^3}$$
$$\hat{k}_\pm = \frac{k_\pm}{k_+}, \qquad \hat{k}_p = \frac{k_p}{k_+}, \qquad \hat{k}_n = \frac{k_n}{k_+}, \qquad \hat{V}_{-,0} = \frac{V_{-,0}}{V_{+,0}}$$

Inserting the dimensionless quantities in equations 1.1, 1.2 and 1.3 yields the dimensionless system of equations

$$n_t = D_0 n_{xx} - (1+k_-)\,n + k_p n_+ + k_n n_- \tag{2.1}$$

$$(n_+)_t + (V_+ n_+)_x = k_+ n - k_p n_+ \qquad x \in [0, L] \tag{2.2}$$

$$(n_-)_t + (V_- n_-)_x = k_- n - k_n n_- \tag{2.3}$$

For a detailed derivation of the dimensionless system of variables see Appendix A

2.2 Initial- and Boundary Conditions

Initially, there will be only free particles, no particles moving along a direction. These free particles are distributed linearly over the domain with their maximum (N_0) at the left boundary and minimum (N_L) at the right boundary.

$$n(x, t=0) = n^0(x) = +\,(N_L - N_0)\,\frac{x}{L} \tag{2.4}$$

$$n_+(x, t=0) = n_+^0(x) = 0 \tag{2.5}$$

$$n_-(x, t=0) = n_-^0(x) = 0 \tag{2.6}$$

Note that the free particles initial condition already fulfills equation 2.1 for a vanishing source term.

The value for free particles is prescribed at both boundaries, consistent with the initial data. For the particles moving in positive direction a Dirichlet boundary condition is set on the left boundary, so that this value can be propagated through the domain. The same accounts for particles moving in negative direction and the right boundary. The boundary conditions read

$$n(x=0,t) = N_0, \quad n(x=L,t) = N_L \tag{2.7}$$
$$n_+(x=0,t) = N_0\sigma_0 \tag{2.8}$$
$$n_-(x=L,t) = N_L\sigma_L \tag{2.9}$$

2.3 Different Hypothesis's for Advective Transport

There are different possible assumptions for modeling the velocity, associated with molecular motors.

The first, and simplest, is to assume constant velocities

$$V_+ = V_{+,0}, \quad V_- = V_{-,0} = -V_{+,0} \tag{2.10}$$

which is reasonable for low concentrations.

A second closure for the velocity is the assumption that the concentration of particles moving along microtubules affects the molecular velocity, as

$$V_+ = V_{+,0}\exp(-An_+), \quad V_- = -V_{+,0}\exp(-An_-) \tag{2.11}$$
$$\text{with: } A > 0$$

The constant motor velocities $V_{+,0}$ and $V_{-,0} = V_{+,0}$ are assumed to be known for small concentrations, according the first assumption. Note that the velocity increases linear for $A = 0$. Figure 2.1 shows the values for V_+ and V_- for $A \in \{0, \dots, 7\}$. The larger the value for A, the smaller the maximum velocity. Note that for small concentrations the velocity of particles increases to then decrease towards zero. The velocity has a maximum, depending on the value of A. This is one possible reason for traffic jams, as the velocity decreases for larger concentrations, resulting in problems to resolve jams.

Their is a third hypothesis regarding mechanisms, that might cause traffic jams. This hypothesis assumes constant velocities, $V_{+,0}, V_{-,0}$, but assumes a non-constant detachment rate for the particles in positive and negative direction.

$$k_p = k_{p,0}\exp(Bn_+), \quad k_n = k_{n,0}\exp(Bn_-) \tag{2.12}$$
$$\text{with: } B(x) = I_{[a,b]}B_0 \tag{2.13}$$

for a subinterval $[a,b]$ in $[0,L]$ and the indicator function $I_{[a,b]}(x)$.

For this work, mainly hypothesis one will be used (see sections 4.1 and 4.2. Section 4.4 will explore the second hypothesis and its effect on the solution.

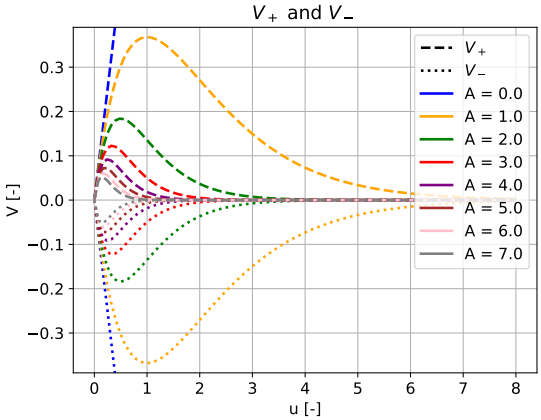

Figure 2.1: The motor velocities increase for small number densities. For increasing number densities the motor velocities decrease towards zero. The larger the parameter A the faster the convergence towards zero. The velocity for $A = 0$ increases linear. The linear model would yields constant velocities V_+, V_-.

2.4 Method of Characteristics

The method of characteristics (MOC) can be utilized to solve an advection equation in terms of an initial-value problem. Uncoupling equation 2.2 from the remaining equations results in

$$(n_+)_t + (n_+)_x = 0 \tag{2.14}$$
$$\Leftrightarrow U_t + U_x = 0 \tag{2.15}$$
$$\text{with: } U(x,0) = U_0(x) \quad \forall x \in \mathbb{R} \tag{2.16}$$

As an ansatz assume that some curve $x(t)$ along the slope of U is constant, meaning

$$0 = \frac{d}{dt}U\left(x(t),t\right) \tag{2.17}$$
$$= U_t\left((x(t),t) + U_x\left(x(t),t\right)\frac{dx}{dt}\right. \tag{2.18}$$

As $U_t + U_x = 0$ (see equation 2.15) $\frac{dx}{dt}$ has to be equal to one to fulfill the partial differential equation. Insert this with

$$\frac{dx}{dt} = 1 \quad \text{with: } x(0) = x_0 \tag{2.19}$$

$$\Rightarrow x(t) = x_0 + t \tag{2.20}$$

resulting in the solution $U(x,t) = U_0(x_0) = U_0(x-t)$ and for the concentrations

$$n_+(x,t) = n_{+,0}(x-t) \tag{2.21}$$

The analytical solution for the uncoupled equation 2.3 can be derived in the same way, resulting in $n_-(x,t) = n_{-,0}(x+t)$. Note that the advection velocity is now $a = -1$, therefore $\frac{dx}{dt} = -1$ has to be fulfilled.

2.5 Discretization with Finite Differences and Upwind Discretization

The coupled system of equations will be solved numerically with the finite-difference scheme and an upwind-discretization for the advective term. In the discrete terms, the upper index $\cdot^j$ indicates the j-th time step, while the lower index $\cdot_i$ indicates the i-th grid point. Δt is the time-step size and Δx the distant between two grid points on an uniform grid.

Discretizing the time with a simple explicit Euler method, the diffusion coefficient with a finite difference stencil of second order and the advective terms with an Upwind discretization, the discretized equations are as follows

$$\frac{n_i^{j+1} - n_i^j}{\Delta t} = D_0 \frac{n_{i+1}^j - 2n_i^j + n_{i-1}^j}{(\Delta x)^2} - (1+k_-)n_i^j + k_p n_{+,i}^j + k_n n_{-,i}^j \tag{2.22}$$

$$\frac{n_{+,i}^{j+1} - n_{+,i}^j}{\Delta t} + \frac{1}{\Delta x}\left(U_{+,i+\frac{1}{2}}^j - U_{+,i-\frac{1}{2}}^j\right) = k_- n_i^j - k_p n_{+,i}^j \tag{2.23}$$

$$\frac{n_{-,i}^{j+1} - n_{-,i}^j}{\Delta t} - \frac{1}{\Delta x}\left(U_{-,i+\frac{1}{2}}^j - U_{-,i-\frac{1}{2}}^j\right) = k_- n_i^j - k_n n_{-,i}^j \tag{2.24}$$

with

$$U_{+,i+\frac{1}{2}}^j = n_{+,i}^j, \quad U_{+,i-\frac{1}{2}}^j = n_{+,i-1}^j \tag{2.25}$$

$$U_{-,i+\frac{1}{2}}^j = n_{-,i+1}^j, \quad U_{-,i-\frac{1}{2}}^j = n_{-,i}^j \tag{2.26}$$

Note that the assumption of constant velocities with their respective values from table 5 is inserted, for the sake of simplicity. Inserting the upwind formulations into the discretized system of equations (2.22-2.24) and reformulating this yields an explicit scheme for time-step $j+1$, depending on time-step j.

$$n_i^{j+1} = n_i^j + \Delta t \left(D_0 \frac{n_{i+1}^j - 2n_i^j + n_{i-1}^j}{(\Delta x)^2} - (1+k_-)n_i^j + k_p n_{+,i}^j + k_n n_{-,i}^j \right) \tag{2.27}$$

$$n_{+,i}^{j+1} = n_{+,i}^j + \Delta t \left(-\frac{1}{\Delta x}\left(n_{+,i}^j - n_{+,i-1}^j\right) + k_- n_i^j - k_p n_{+,i}^j \right) \tag{2.28}$$

$$n_{-,i}^{j+1} = n_{-,i}^j + \Delta t \left(+\frac{1}{\Delta x}\left(n_{-,i+1}^j - n_{-,i}^j\right) + k_- n_i^j - k_n n_{-,i}^j \right) \tag{2.29}$$

which is straight forward to implement in Python with the numpy library, in the case of homogeneous Neumann boundary conditions, as they will be used in this work. A for-loop over all time steps has to be implemented and for each time-step the explicit update, following equations 2.27-2.29, has to be called. The implementation is slightly different as equations 2.27-2.29; first an intermediate value for $n_i^{j+1}, n_{+,i}^{j+1}, n_{-,i}^{j+1}$ is computed, based only on the finite difference approximation, without the coupling conditions. After this, the coupling is done, based on the intermediate values. In the last step the Dirichlet boundary conditions can be enforced by setting the boundary points $n_0^{j+1}, n_m^{j+1}, n_{+,0}^{j+1}, n_{-,m}^{j+1}$ to their respective value.

2.6 Stability Criteria

As the numerical scheme is of an explicit form, it is not unconditionally stable. For the L^1-estimate, to fulfill conservation of the concentrations n, n_+, n_-, the scheme has to fulfill

$$\int_0^1 |u(x,t)|dx \leq \int_0^1 |u_0(x)|dx \tag{2.30}$$

or in the discretized formulation

$$\sum_{j=1}^{M} |u_j^{n+1}|\Delta x \leq \sum_{j=1}^{M} |u_{0,j}|\Delta x \quad \Leftrightarrow \sum_{j=1}^{M} |u_j^{n+1}| \leq \sum_{j=1}^{n} |u_j^n| \tag{2.31}$$

For the two uncoupled advection equations under the assumptions of a uniform advection velocity a=1 this results in the following derivation.

With the triangular inequality ($|a+b| \leq |a| + |b|$) and $\lambda = \frac{\Delta t}{\Delta x}$ the concentration at the next time step can be reformulated to

$$\left|u_j^{n+1}\right| = \left|u_j^n - \lambda(u_j^n - u_{j-1}^n)\right| \leq (1-\lambda)\left|u_j^n\right| + \lambda\left|u_{j-1}^n\right| \tag{2.32}$$

under the constraint $1 - \lambda \geq 0$. Tis discretized concentration can be inserted into equation 2.31 to get

$$\sum_{j=1}^{M}\left|u_j^{n+1}\right| \leq (1-\lambda)\sum_{j=1}^{M}\left|u_j^n\right| + \lambda\sum_{j=1}^{M}\left|u_{j-1}^n\right| \tag{2.33}$$

$$= (1-\lambda)\sum_{j=1}^{M}\left|u_j^n\right| + \lambda\sum_{j=1}^{M}\left|u_j^n\right| \tag{2.34}$$

$$= \sum_{j=1}^{M}\left|u_j^n\right| \tag{2.35}$$

Therefore, the discretization for the advection equation is stable under the condition

$$1 - \lambda = 1 - \frac{\Delta t}{\Delta x} \geq 0 \tag{2.36}$$

$$\Leftrightarrow \frac{\Delta t}{\Delta x} \leq 1 \tag{2.37}$$

For general advection equation ($a = a$) the stability constraint is called the CFL-condition and reads:

$$a\frac{\Delta t}{\Delta x} \leq 1 \tag{2.38}$$

For the diffusion equation a similar derivation can be performed, resulting in the more strict constraint

$$D_0\frac{\Delta t}{(\Delta x)^2} \leq \frac{1}{2} \tag{2.39}$$

3 Implementation

All the following examples, visualizations and the discussed implementation can be found in the reproducability repository for this project (see [1]). All the implementations are done with the Python programming language, mainly with the numpy package for vector operations and matplotlib for visualizations. Furthermore, there is an additional implementation using the open-source software FEniCSx[1], which utilizes the Finite Element Method. This software was used to check the Python implementation and the correctness of the method.

3.1 Convergence Analysis

A convergence analysis was performed to ensure the numerical implemenation's correctness for the two uncoupled advection equations. The solutions for different grid sizes are compared to the analytical solution. To interpret the convergence of the numerical method, a relevant error measure is introduced. The $\mathcal{L}_1$ norm and its relative counterpart are calculated as

$$\mathcal{L}_1(u) = \int_\Omega |u - u_{\text{exact}}|\, d\Omega \tag{3.1}$$

$$\mathcal{L}_{1,\text{rel}}(u) = \frac{\mathcal{L}_1(u)}{\int_\Omega |u_{\text{exact}}|\, d\Omega} \tag{3.2}$$

For the convergence analysis, the relative error norm $\mathcal{L}_{1,\text{rel}}$ with the default parameter (see Table 5) will be used. The grid length is chosen from $\Delta x \in \{2.0, 0.2, 0.02, 0.002\}$ at $t = 10$. The cfl-condition was checked for every grid size. If the condition was not fulfilled, the time step size was reduced iteratively, until it was fulfilled.

Figure 3.1 visualizes the $\mathcal{L}_{1,\text{rel}}$ error for both, the particles moving in positive and negative direction. Note that both axis are scaled logarithmic. Both error converge approximately with an order which is somewhat below first order. As the used finite difference stencil for the spatial derivative $(n_\pm)_x$ is of first order, this is not the theoretical best convergence, but it is sufficient for a rather rudimentary implementation. As the initial condition for the diffusion equation already satisfies the diffusion equation, the numerical solution will fulfill the analytical solution at all times.

1. FEniCSx: https://fenicsproject.org/

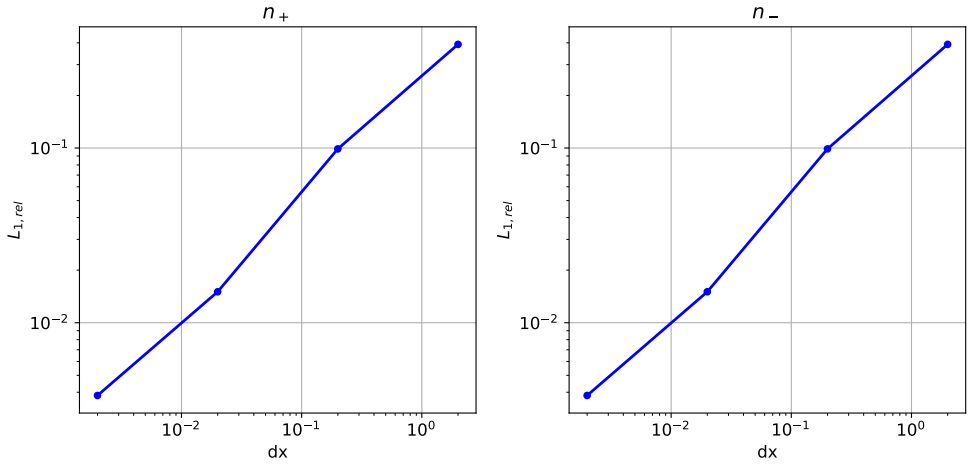

Figure 3.1: The numerical scheme converges with an order somewhat below first order for both, the particles moving in positive and negative direction. The x-axis shows the grid length in dimensionless units and the y-axis the $\mathcal{L}_{2,\text{rel}}$ error. Both axis are scaled logarithmic. Note that the initial solution for the uncoupled diffusion equation already fulfills the analytical solution and is therefore dropped in this analysis.

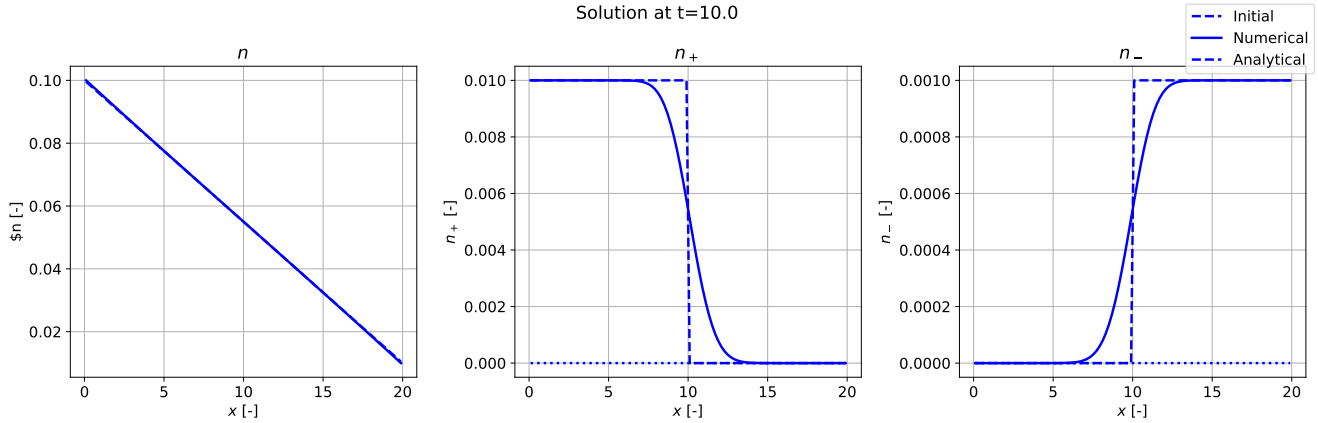

Figure 4.1: The free particles already fulfill the diffusion equation at all times, while the particles moving along one direction are propagated from the Dirichlet boundary towards the domain. This propagation results in a shock at $x = t$, as the advection velocity has the value 1. The x-axis shows the spatial domain while the y-axis shows the concentration for free particles (left), particles moving in positive direction (center) and particles moving in negative direction (right) at time $t = 10$. The initial values are visualized with dotted lines, the numerical with solid lines and the analytical with dashed lines.

4 Results

In the following the numerical approximations for the system will be discussed. First, the uncoupled system will be taken into account to then slowly increase the complexity, ending in the fully coupled system with an additional hypothesis for the advective transport (see [2]).

4.1 Uncoupling the System

Consider the uncoupled system of equations

$$n_t = D_0 n_{xx} \tag{4.1}$$

$$(n_+)_t + (n_+)_x = 0 \tag{4.2}$$

$$(n_-) - (n_-)_x = 0 \tag{4.3}$$

with the analytical solutions for equations 4.2 and 4.3, as found in section 2.4.

Figure 4.1 visualizes the state of the different concentrations at $t = 10$. The free particle concentration (n) is the same as initially, as this already fulfills the Diffusion equation. The concentrations of particles moving in positive (n_+)

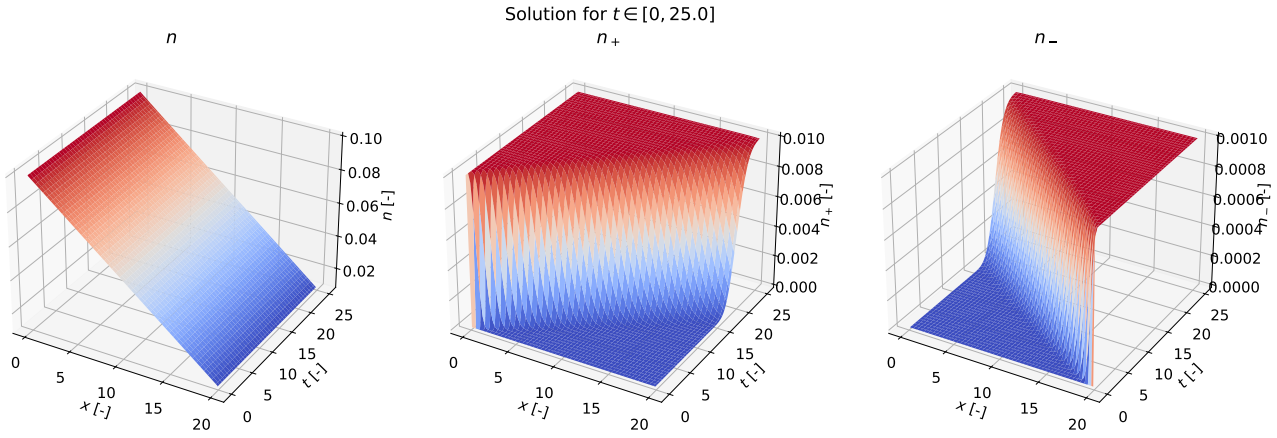

(a) The free particles' concentration is constant over the time frame. The number densities of particles attached to molecular motors are propagated and result in a constant solution over the whole spatial domain.

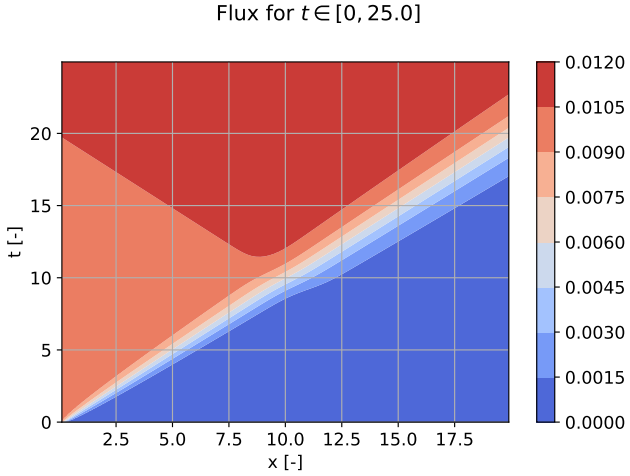

(b) On the left, the flux increases faster then on the right, as the number density of particles moving in positive direction is higher as the number density of the particles moving in negative direction. At roughly $t = 10$ the shocks of both species meet around $x \approx 10$ and the flux has reached its maximum on the center of the domain, increasing towards its stationary value on the boundaries.

Figure 4.2: The numberical solution converges towards the stationary solution after approximately 21.85 dimensionless time units. At this time, the number densities for particles moving along a direction are constant over the whole domain and the flux is constant, too.

and negative (n_-) direction are propagated, starting at the Dirichlet boundary, with an advection speed of 1. Therefore, the analytical solution shows a shock at $x = t$ from the Dirichlet boundary value to the initial value zero. The finite difference scheme is not capable to capture this discontinuity, as it is only a method of first order discretized in time with an explicit Euler. Therefore, the numerical solution shows some error close to the shock.

As the concentration is propagated with a propagation speed of 1 over a domain of length 20, it takes 20 dimensionless time units to fully propagate from one boundary to the other.

Figure 4.2a shows the three different concentrations for $t \in [0, 25]$, calculated numerically. The numerical solution needs longer to be fully propagated, due to the numerical error. However, after 21.85 time units, the numerical solution is fully propagated, resulting in the stationary solution for $t > 21.85$.

Summing up equations 2.1-2.3 results in

$$(n + n_+ + n_-)_t + \underbrace{(n_+ - n_- - D_0 n_x)}_{J})_x = 0 \tag{4.4}$$

Where $n_+ - n_- - D_0 n_x$ is the total flux J. This total flux should will vary initially and result in a constant solution after the different concentrations reached the stationary behavior. The total mass will reach its stationary solution at the same time as the total flux, namely $t = 20$ analytically and $t = 21.85$ numerically.

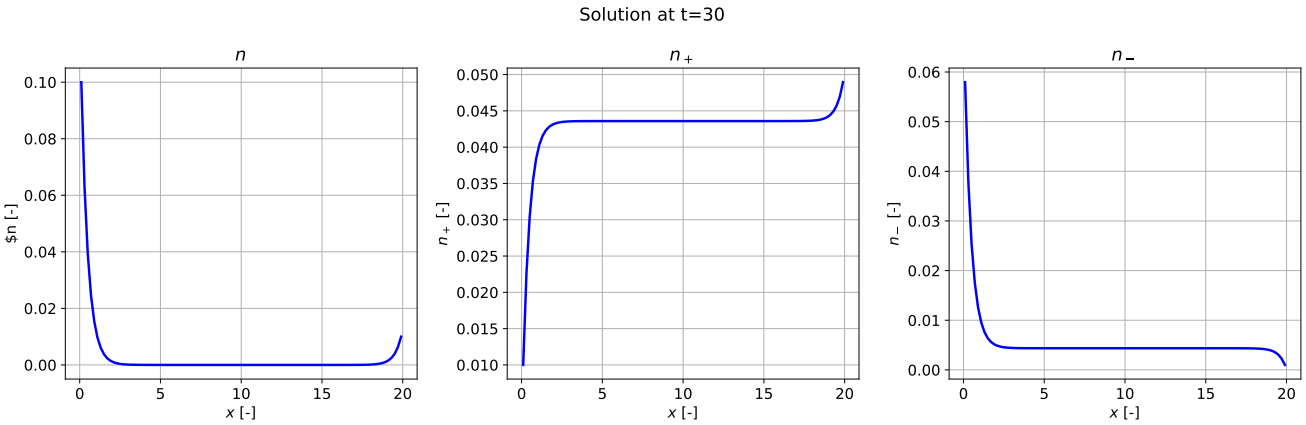

(a) The visualized time is $t = 30$, showing the stationary case. The free particles converge towards zero on a major part of the domain for the stationary case. The particles moving in positive direction increase exponentially at their Dirichlet boundary and are constant on a major part of the remaining domain. The particles moving in negative direction show a similar behavior, just with a smaller concentration and a larger increase at the non Dirichlet boundary. The larger increase for particles attached to molecular motors at the left boundary is in accordance with the free particles and their Dirichlet boundary values.

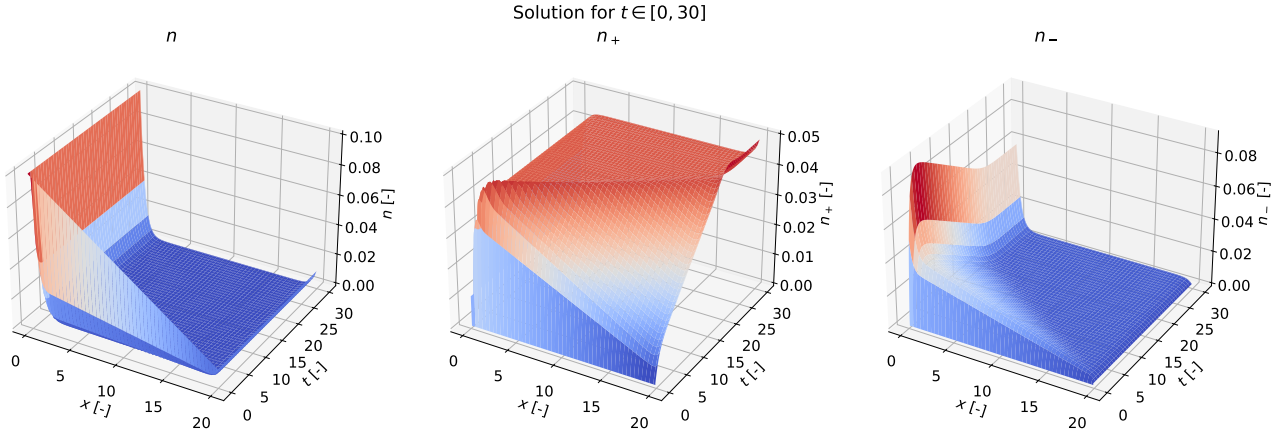

(b) The free particles reach there stationary state very fast, while the particles moving along with molecular motors need longer to do so.

Figure 4.3: Adding the coupling of free particles results in a domain with almost no free particles and mainly advective particles.

4.2 Increasing the Complexity by Adding Source Terms

4.2.1 Coupling of Free Particles

As a next step, the source terms will be partly integrated into the system. First, consider the uncoupled system with source terms connecting the free particles, resulting in

$$n_t = D_0 n_{xx} - (1 + k_-)n \tag{4.5}$$

$$(n_+)_t + (n_+)_x = n \tag{4.6}$$

$$(n_-) - (n_-)_x = k_- n \tag{4.7}$$

The term $-(1+k_-)n$ in equation 4.5 models the loss of free particles towards particles moving along one direction. As these particles are added towards the moving particles along a traction, they are also added to the right-hand-side of equation 4.6 (n) and equation 4.7 ($k_- n$).

Figure 4.3 visualizes the concentrations (y-axis) over the spatial domain (x-axis) for the three different concentrations, according to this simple coupling for $t \in [0, 10]$.

The free particles concentration starts to change over time, as it loses particles to the other types. After just a few iterations, there are no free particles left in the center of the domain and the free particle concentration increases towards their Dirichlet values close to the boundaries. The particles moving with molecular motors into positive direction converge towards their stationary behavior, with an exponential increase in concentration at the left boundary to a value of 0.044 on a large part of the domain and then increases towards its maximum value at the right boundary. The particles moving in negative direction show a similar behavior with an exponential loss at the left boundary towards a value of 0.005 to then decrease at the right boundary towards their Dirichlet value 0.001.

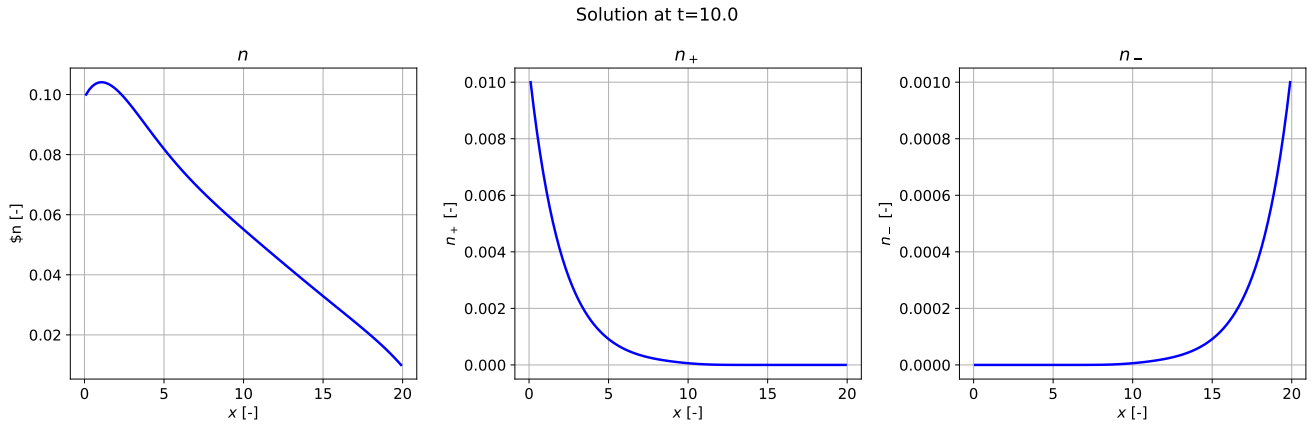

(a) The visualized time is $t = 10$, showing the stationary case. The number density of free particles increases, due to the gain in particles from the coupling. These particles show a local maximum at the left side, as the particles moving in positive direction have a higher concentration compared to the particles moving in negative direction. this results in a larger exchange at the left side. The number densities of particles moving along with molecular motors converges towards zero at their non Dirichlet boundary, with an exponential decrease from the Dirichlet boundary value.

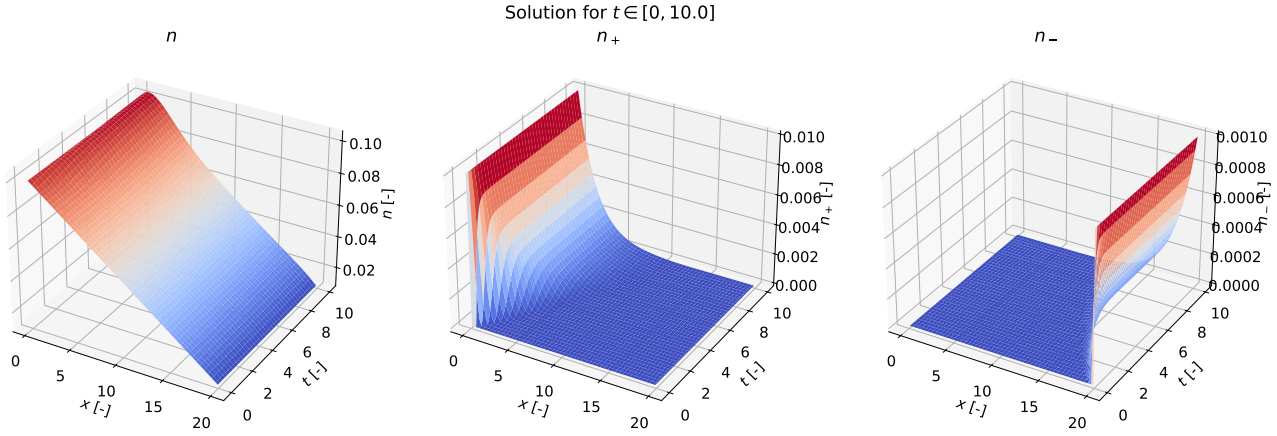

(b) Adding the coupling of advective particles results in a rather fast convergence towards the stationary solution. The free particles show a slight shift from their initial solution, while the particles moving along molecular motors show a major change to the previous solutions.

Figure 4.4: Adding the coupling of particles attached to molecular motors results in an increase in free particles over the domain, with a peek at the left side. The particles attached to molecular motors show an exponential decrease from their Dirichlet boundary towards zero.

4.2.2 Coupling of Particles Moving with Molecular Motors

Next, only consider coupling conditions for particles moving along one direction, resulting in

$$n_t = D_0 n_{xx} + k_p n_+ + k_n n_- \tag{4.8}$$

$$(n_+) + (n_+)_x = -k_p n_+ \tag{4.9}$$

$$(n_-) - (n_-)_x = -k_n n_- \tag{4.10}$$

The particles moving with a velocity now lose particles to the free particles with the factor (k_p, k_n).

The increase in concentration for the free particles can be seen in Figure 4.4, mainly at the left side of the domain for the free particles, where a local maximum in free particles forms. The concentration of particles moving with molecular motors decreases exponentially to zero, starting from their Dirichlet boundary value. Therefore, no particles moving in positive direction will reach the right boundary and no particles moving in left direction will reach the left boundary. Before, they will attach to the diffusive behavior and convert to free particles.The peek of free particles on the left of the domain is due to the maximum of particles moving in positive direction on the left side being one order higher then the maximum of particles moving in negative direction on the right.

4.3 Fully Coupled System of Intercellular Transport in Axons with a Constant Velocity

Consider the fully coupled system (equations 2.1-2.3) with the hypothesis of constant velocities ($V_+ = V_{+,0}, V_- = V_{-,0} = -V_{+,0}$). For this system, free particles attach to molecular motors and vice versa.

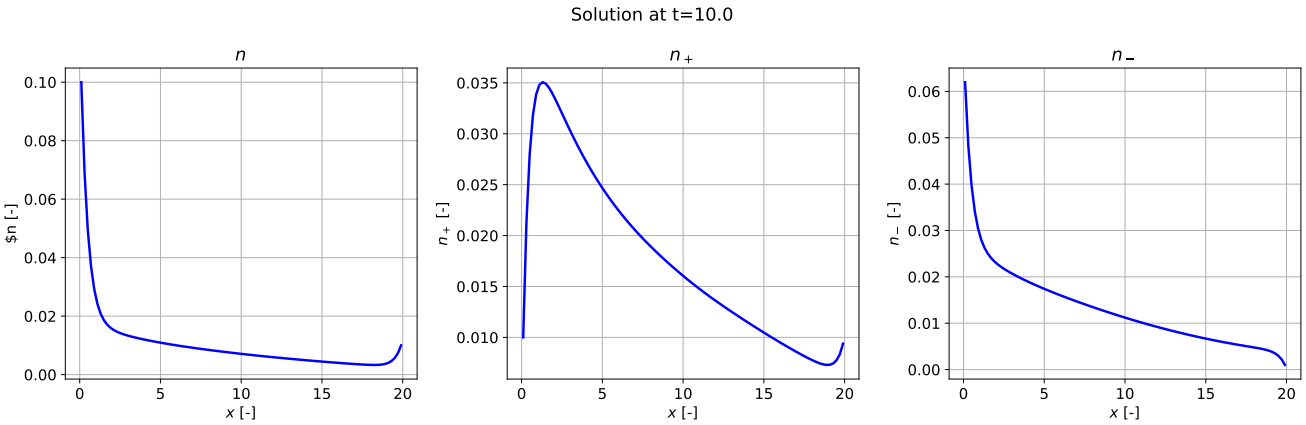

(a) The visualization shows the fully coupled system at time step $t = 10$. The free particles' concentration decreases on the interior of the domain, not going towards zero, with a smaller concentration on the right. The particles moving in positive direction show a slight traffic jam at the left side, which is resolved on the remaining domain. The particles moving in negative direction show an exponential increase on both boundaries, with an almost linear behavior on the interior of the domain.

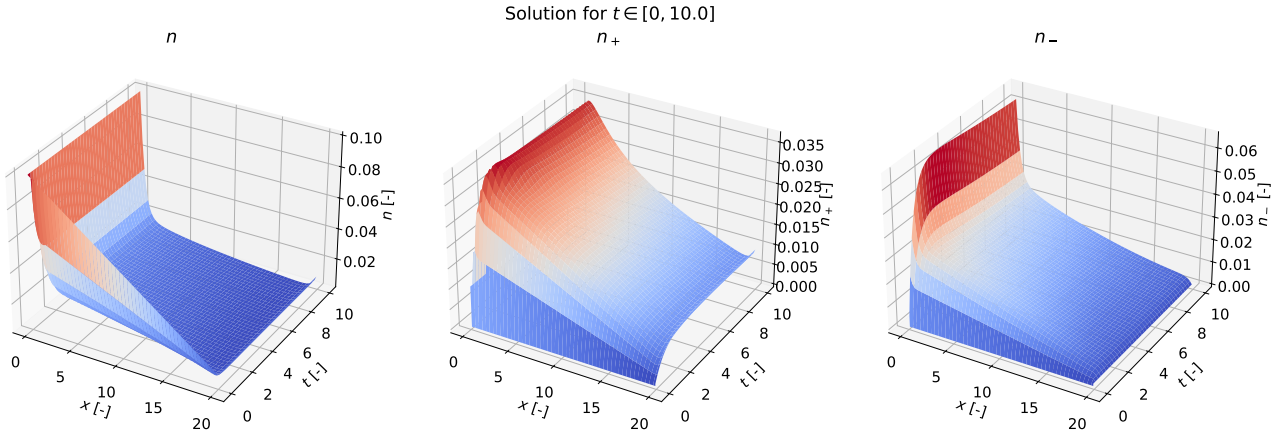

(b) The fully coupled system reaches its stationary behavior very fast, compared to the simplified systems.

Figure 4.5: Solving the fully coupled system of equations with constant velocities results in a traffic jam for particles moving in positive direction.

The behavior of the free particles is similar to section 4.2.1. However, there is a positive concentration over the whole domain with its smallest value close to the right boundary. Further, the particles moving towards the neuron body (n_-) have its minimum at their right boundary and then strictly increase towards their maximum at the left boundary. Close to the boundary, their is a sharp increase. This increase is explainable with the behavior of the particles moving away from the neuron body (n_+). These particles form a traffic jam close to the left boundary ($\sim x = 2$) with a maximum number density $\max(n_+) \approx 0.035$. This traffic jam is then resolved over the remaining part of the domain.

4.4 Fully Coupled System of Intercellular Transport in Axons with a Nonlinear Velocity Profile

Consider the same system as in section 4.3, but with the nonlinear velocity profile presented in equation 2.11.

$$V_+ = V_{+,0} \exp(-An_+), \quad V_- = -V_{+,0} \exp(-An_-)$$
$$\text{with: } A > 0$$

This velocity profile slows down the velocity, if the number density increases (compare with Figure 2.1). Furthermore, a larger value for A leads to a smaller velocity, which then increases the maximum number density, making the traffic jam even worse.

Figure 4.6 visualizes the effect of A (for $A \in [0, \ldots, 7]$) on the number densities of the different species. The advection velocity has almost no effect on the free particles concentration, while it has a large effect on the number density of particles moving in positive direction, as discussed above. The larger the value for A, the smaller the total maximum of particles moving in negative direction (at the left boundary). Besides this, the concentration of these particles differs at the point of the traffic jam, depending on A, but on the remaining domain there is almost no difference over the different values of A.

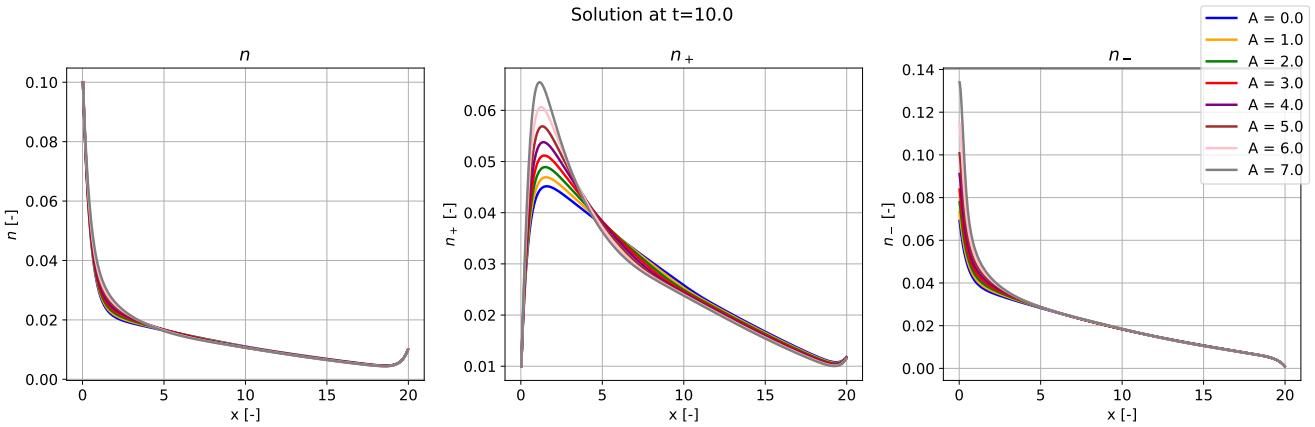

Figure 4.6: The nonlinear velocities yield the same qualitatively solution as the fully coupled system with linear velocities. However, it shows quantitatively different solutions for different values of A. The free particles concentration is almost not influenced by the parameter A. The particles moving along molecular motors in negative direction yield a different boundary value at the left. The larger A, the larger this boundary value. Further, the significance of the traffic jam increases for increasing values of A

The qualitatively solution can be verified with existing literature (compare with Figure 2 from [2]). However, the values of the maxima have a certain offset. It can be shown, that the solution converges towards the correct solution for a refined mesh. However, the current Python implementation lacks an efficient implementation in terms of memory usage and efficiency, resulting in the need of a rather coarse mesh ($\Delta x = 0.05$) to solve the system efficiently.

5 Discussion and Conclusion

To sum it up, traffic jam situations can occur in axons under the assumption of a coupling between the diffusive and advective transport. The linear model approximates this traffic jam situation qualitatively, but quantitatively there are differences to the nonlinear velocity model for different nonlinear parameter A.

Traffic jam situations, where particles accumulate along the spatial domain and hinder an efficient transport mechanism mainly occur when these particles do not move fast enough or these accumulated particles are not converted to other particles fast enough. Therefore, a smaller advection velocity at higher number densities is a major problem, as the formation of traffic jams is supported by this. However, if the exchange of particles can be increased at higher number densities, this can help to prevent and break traffic jams.

From a medical point of view two different approaches are interesting:

1) Medicine that increases the particles overall velocity and the velocity of particles for the situation of a high number density
2) Medicaments that increase the particle loss, if the number density increases.

For future work it will be interesting to implement the third closure for the velocities into the existing Python framework and check its performance. Further, the influence of different parameter on the significance of traffic jams can be analyzed in a parameter study.

List of Variables

All the variables, listed in the following table, are in their dimensionless form.

DIMENSIONLESS VARIABLES

Variable	Default Value	Property
L	20	Axon length
N_0	0.1	Diffusion coefficient
N_L	0.01	Concentration of free particles at left boundary
k_-	1	Concentration of free particles at right boundary
σ_0, σ_L	$0.1, 0.1$	binding rate in negative direction
k_p, k_n	0.5	Degree of loading at left and right boundary
Δx	0.2	Detachment rate for particles in positive and negative direction
t_{end}	10	Grid length
N_{time}	200	Number of time steps
Δt	0.05	Time step size

INDEXING

Variable	Meaning
$\cdot^j$	j-th time step
$\cdot_i$	i-th grid point

REFERENCES

[1] Jan Habscheid. Reproducibility repository for data-driven modeling of conservation laws, February 2025. URL: https://git.rwth-aachen.de/JanHab/ddm.

[2] A.V. Kuznetsov and K. Hooman. Modeling traffic jams in intracellular transport in axons. *International Journal of Heat and Mass Transfer*, 51(23):5695–5699, 2008. Biomedical-Related Special Issue. URL: https://www.sciencedirect.com/science/article/pii/S0017931008002731, doi:10.1016/j.ijheatmasstransfer.2008.04.022.

APPENDIX

Inserting the dimensionless variables

$$\hat{x} = \frac{xk_+}{V_{+,0}}, \qquad \hat{t} = tk_+, \qquad \hat{D}_0 = \frac{D_0 k_p}{V_{+,0}^2}, \qquad \hat{n} = \frac{nV_{+,0}^3}{k_+^3}, \quad n_\pm = \frac{\hat{n}_\pm V_{+,0}^3}{k_\pm^3}$$
$$\hat{k}_\pm = \frac{k_\pm}{k_+}, \qquad \hat{k}_p = \frac{k_p}{k_+}, \qquad \hat{k}_n = \frac{k_n}{k_+}, \qquad \hat{V}_{-,0} = \frac{V_{-,0}}{V_{+,0}}$$

in equations 1.1-1.3 yields the dimensionless system of equations 2.1-2.3.

First, insert the respective dimensionless variables in equation 1.1.

$$\begin{aligned}
\hat{n}_{\hat{t}} &= \hat{D}_0 \hat{n}_{\hat{x}\hat{x}} - (1+\hat{k}_-)\hat{n} + \hat{k}_p \hat{n}_+ + \hat{k}_n \hat{n}_- \\
\Leftrightarrow \underbrace{\frac{nV_{+,0}^3}{k_+^3}}_{tk_+} &= \frac{D_0 k_+}{V_{+,0}^2} \underbrace{\frac{nV_{+,0}^3}{k_+^3}}_{\frac{xk_+}{V_{+,0}}\frac{xk_+}{V_{+,0}}} + \frac{k_p}{k_+}\frac{n_+ V_{+,0}^3}{k_+^3} + \frac{k_n}{k_+}\frac{n_- V_{+,0}^3}{k_+^3} \\
\Leftrightarrow n_t \frac{1}{k_+} &= \frac{D_0 k_+}{V_{+,0}^2} n_{xx} \frac{V_{+,0}^2}{k_+^2} + \frac{k_p}{k_+} n_+ + \frac{k_n}{k_+} n_- \\
\Leftrightarrow \frac{n_t}{k_+} &= \frac{D_0 n_{xx}}{k_+} + \frac{k_p n_+}{k_+} + \frac{k_n}{k_+} n_- \\
\Leftrightarrow n_t &= D_0 n_{xx} + k_p n_+ + k_n n_-
\end{aligned}$$

Note that this is the proposed dimensionless equation for free particles. Second, insert the dimensionless variables in equation 1.2.

$$(\hat{n}_+)_{\hat{t}} + \left(\frac{V_+}{V_{+,0}}\hat{n}_+\right)_{\hat{x}} = \hat{k}_+ \hat{n} - \hat{k}_p \hat{n}_+ \tag{A.1}$$

$$\underbrace{\left(\frac{nV_{+,0}^3}{k_+^3}\right)}_{tk_+} + \underbrace{\left(\frac{V_+}{V_{+,0}}\frac{nV_{+,0}^3}{k_+^3}\right)}_{\frac{xk_+}{V_{+,0}}} = \frac{k_+}{k_+}\frac{nV_{+,0}^3}{k_+^3} - \frac{k_p}{k_+}\frac{n_+ V_{+,0}^3}{k_+^3} \tag{A.2}$$

$$\Leftrightarrow \left(\frac{nV_{+,0}^3}{k_+^3}\right) + \left(\frac{V_+ V_{+,0}^3 n}{k_+^4}\right)_x = n\frac{V_{+,0}^3}{k_+^3} - nk_p\frac{V_{+,0}^3}{k_+^4} \tag{A.3}$$

This yields equation 2.2. The dimensionless form of equation 1.3 can be derived in the same way, as it is of the same form as shown above.